Hadronic structure, low x physics and diffraction

P. Marage

Université Libre de Bruxelles - CP 230, Boulevard du Triomphe, B-1050 Bruxelles, Belgium
E-mail: pmarage@ulb.ac.be

Abstract
A review is presented of numerous recent results, particularly those submitted to the EPS-HEP99 conference: very high Q^2 ep interactions and direct tests of the Standard Model, new measurements of the structure of the proton (including high x parton distributions and tests of QCD involving the gluon distribution), low x physics (tests of the BFKL evolution), diffraction in DIS at HERA, hard diffraction at the Tevatron and exclusive production of vector particles at HERA. The focus is on hard QCD features †.

1. Introduction.

The present review covers a very large field of research, illustrated by over 80 papers submitted to this conference, including results form HERA, the Tevatron and fixed target experiments. After a presentation of direct tests of the Standard Model (SM) performed at HERA at very high Q^2, the focus of the paper is on hard QCD features †.

Time has gone when QCD needed to be tested as the theory of strong interactions. The task is now to improve our understanding of the theory, i.e. provide a consistent and detailed QCD description of fundamental features of particle physics, in particular the structure of hadrons and diffractive scattering, and evaluate the validity of different approximations and calculation techniques.

2. The proton at the 10^{-3} fm scale.

A highlight of this conference is the presentation by the H1 and ZEUS experiments at HERA of measurements of the proton structure for $Q^2 \gtrsim M_Z^2$, i.e. at a scale of 10^{-3} fm [4, 5]. These results were obtained from the scattering of 27.5 GeV positrons with 820 GeV protons ($\sqrt{s} = 300$ GeV, 40 pb^{-1} data taken in 1994-97) and of 27.5 GeV electrons with 920 GeV protons ($\sqrt{s} = 320$ GeV, 16 pb^{-1} data taken in 1998-99), both in neutral current (NC) and charged current (CC) interactions. They confirm, in a widely extended kinematic domain, the validity of the SM [6].

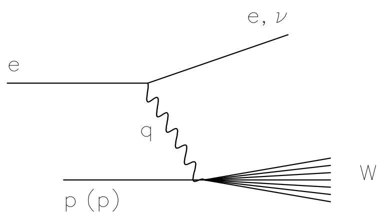

Figure 1. Deep inelastic ep scattering.

The kinematics of ep deep inelastic scattering (DIS) is sketched on Fig. 1. The following variables are used: $Q^2 = -q^2; x = Q^2/2p \cdot q; W^2 \simeq Q^2/x; y \simeq Q^2/x \cdot s$. The variable x is, in the Breit frame, the fraction of the proton momentum carried by the struck quark; W is the invariant mass of the hadronic system; $\sqrt{s}$ is the ep centre of mass system (cms) energy.

In the SM, the cross section for DIS ep scattering is given in terms of the F_2, F_L and F_3 structure functions in the following forms:

- *NC*

$$\frac{\mathrm{d}^2\sigma^{NC}}{\mathrm{d}x\,\mathrm{d}Q^2} = \frac{2\pi\alpha^2}{x\,Q^4}\,[Y_+\,F_2(x,Q^2) \\ -y^2\,F_L(x,Q^2) \mp Y_-\,xF_3(x,Q^2)], \qquad (1)$$

where α is the fine structure coupling constant and $Y_\pm = 1 \pm (1-y)^2$; the $-$ sign in front of the electroweak contribution proportional to xF_3 is for e^+ scattering and the $+$ sign for e^-.

- *CC*

[1] Plenary report presented at the International Europhysics Conference on High Energy Physics, EPS-HEP99, Tampere, Finland, 15-21 July 1999.

[2] By lack of time and space, numerous interesting and important topics could not be covered by the present report, in particular hadron final state in DIS and diffraction [1], leading baryon studies [2], spin physics [3].

$$\frac{\mathrm{d}^2\sigma^{CC}}{\mathrm{d}x\,\mathrm{d}Q^2} = \frac{G_F^2}{4\pi x}\,(\frac{M_W^2}{M_W^2+Q^2})^2\,[Y_+\,F_2(x,Q^2) \\ -y^2\,F_L(x,Q^2) \mp Y_-\,xF_3(x,Q^2)]. \qquad (2)$$

It is useful to get rid of the trivial x and Q^2 dependences in relations (1) and (2), and to define "reduced" cross sections $\tilde{\sigma}$ corresponding to the quantities between brackets (see [4,5]).

Fig. 2 presents measurements of the e^+p and e^-p NC and CC cross sections [4]. The similarity of the NC and CC cross sections for $Q^2 \approx M_Z^2$ demonstrates electroweak unification in the t channel.

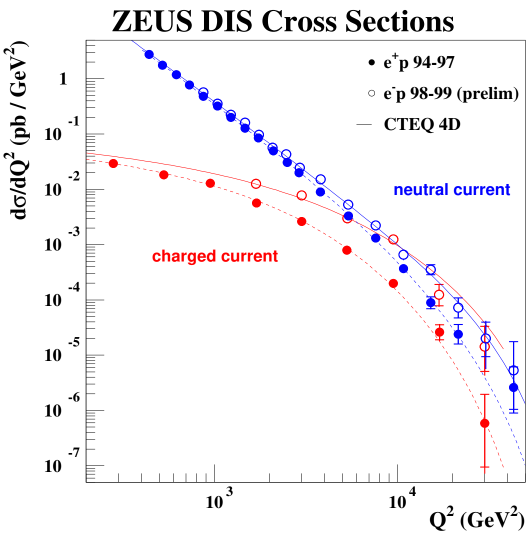

Figure 2. ZEUS measurements of e^+p and e^-p NC and CC cross section measurements, as a function of Q^2 [4]. The lines represent the SM predictions using the CTEQ4D parton distribution functions (pdf's).

Parity violation effects due to the electroweak contribution ($\gamma - Z^\circ$ interference) and corresponding to the change of sign in relation (1) are visible from the difference between the e^+p and e^-p NC cross sections at high Q^2 (see Fig. 3; the effect of the small difference in $\sqrt{s}$ is negligible).

The helicity structure of the interaction is directly visible from the y dependence of the CC cross sections, shown in Fig. 4. The cross section for CC e^-p interactions is proportional to $[u+c]+(1-y)^2[\bar{d}+\bar{s}]$, where q represents the density distribution of quark q in the proton. It is dominated by u quarks, and is thus large and weakly dependent on $(1-y)^2$. In contrast, the CC e^+p cross section is proportional to $[\bar{u}+\bar{c}]+(1-y)^2[d+s]$, thus proportional to $(1-y)^2$ with a small intercept. The contribution of d quarks at high x can be seen in Fig. 5, which presents the e^+p CC cross section measurement as a function of x in bins of Q^2.

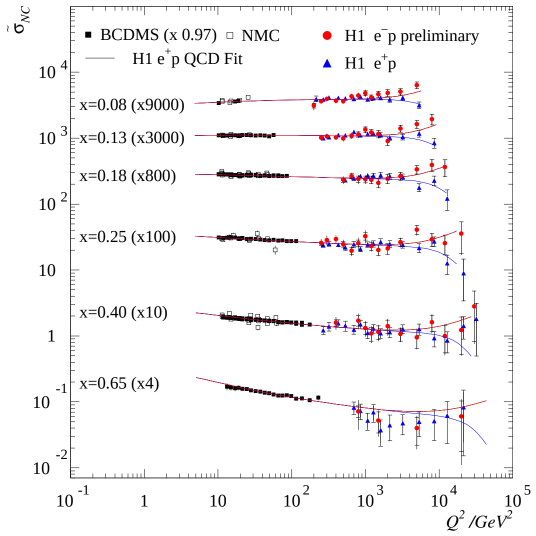

Figure 3. H1 measurement of e^+p and e^-p NC cross sections, exhibiting the effects of parity violation at high Q^2 values [5].

In conclusion, HERA has reached the space-like $Q^2 \simeq M_Z^2$ region with a measurement at the 20% precision level of the e^+ and e^- CC and NC cross sections. This allows the direct observation of the electroweak unification, of parity violation effects in NC and of the quark helicity structure.

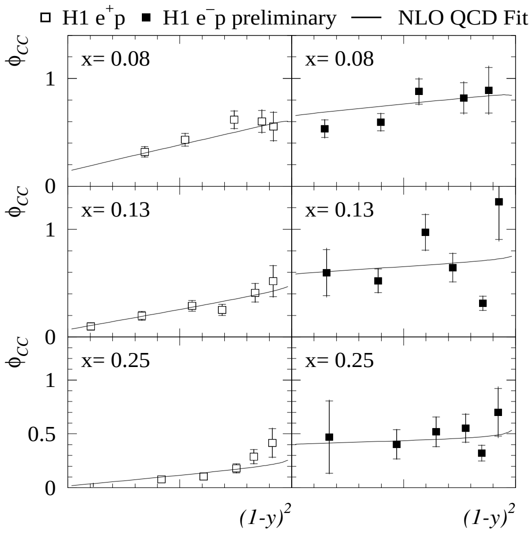

Figure 4. H1 measurements of the y dependence of the e^+p and e^-p CC reduced cross sections [5].

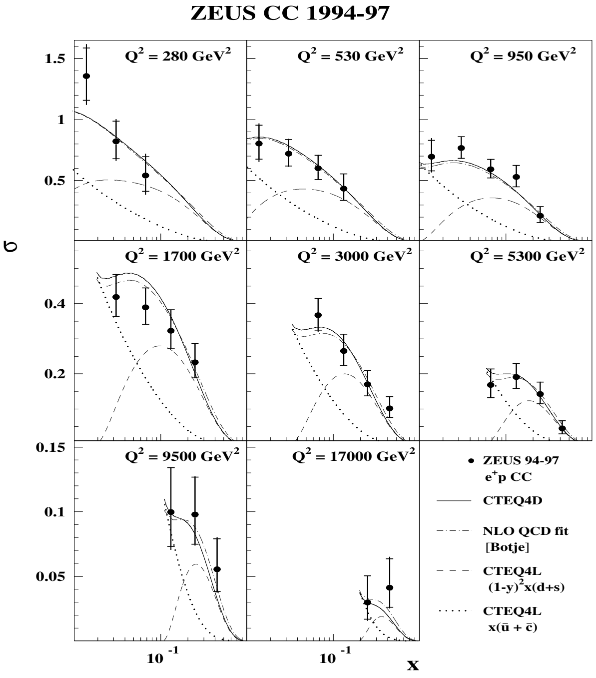

Figure 5. ZEUS measurements of the e^+p reduced cross section $\tilde{\sigma}$ as a function of x in bins of Q^2 [4]. The solid lines represent the SM predictions using the CTEQ4D pdf's. The dashed and dotted lines represent the $d+s$ and $\bar{u}+\bar{c}$ contributions, respectively (CTEQ4L pdf's).

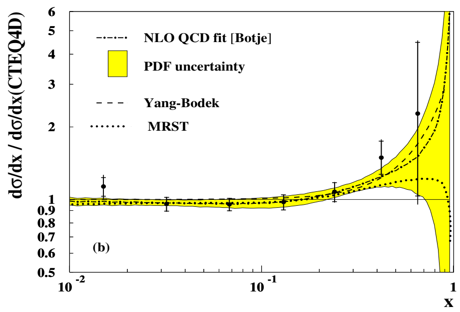

Figure 6. Ratio of the ZEUS measurement of the e^+p CC cross section to the SM expectation using the CTEQ4D pdf's [4]. The dashed-dotted line is a NLO QCD fit [10]; the associated pdf uncertainties are shown as the shaded band. The dashed line is the expectation for the modified d/u ratio [16].

3. The structure of the proton.

Understanding the structure of hadrons, in particular the proton, is one of the main goals of particle physics but the task is difficult since it implies the description of long distance, non-perturbative effects. Fortunately, factorisation applies in DIS between parton distribution functions (pdf's) in the target hadron (proton) and hard processes involving short distance interactions of partons.

The parameterisation of the pdf's and the study of their evolution according to the interaction scale provide information both on the proton structure and on the relevant features of QCD. Their precise determination is also the base-line for any investigation of new physics.

The functional form of the pdf's is not known theoretically. Empirical parameterisations, guided by theoretical arguments, are thus used. In order to reduce the number of free parameters, additional conditions are imposed, mainly constraining relations between different sea quark density distributions and between sea quark and gluon distributions.

Modern parameterisations of pdf's [7–12] share common features:

- the use of NLO DLGAP [13] evolution equations;
- a starting scale $Q^2_\circ = 1-2\ \mathrm{GeV}^2$ (or even lower [7]) for the QCD evolution;
- the dynamical inclusion of heavy quarks [14, 15], needed since $Q^2_\circ < m^2_c$;
- the use of essentially the same data sets.

Differences between parameterisations concern mainly:

- the choice of pdf's at the starting scale $Q^2_\circ$ (different functional forms and constraints);
- details of the choice of data and cuts;
- the choice of SM parameter values (α_s);
- details of the inclusion of heavy quarks.

It should be stressed that the errors on the fitted pdf's are not well known, which limits the significance of comparisons between theoretical predictions and data. The difficulty in asserting errors on pdf's arises from the difficulty in controlling the following effects, several of which are addressed in the course of the present talk:

- the choice of experimental data (data of poor precision, conflicting results);
- the treatment of experimental errors in the data (correlated systematic errors);
- the freedom of choice of the starting parameterisation form;
- theoretical uncertainties (higher order effects, non DGLAP evolution, higher twist contributions, nuclear effects).

In the low and intermediate x regions, the quark distributions are well known thanks to DIS and Drell-Yan measurements; the precision is lower for the gluon distribution since gluons are not directly probed in DIS. At higher x, the d quark distribution for $x \gtrsim 0.5$ (see Fig. 6) and the gluon distribution for $x \gtrsim 0.1$ are rather poorly known.

3.1. High x parton distributions.

3.1.1. The d/u ratio. The measurement of the d/u ratio of valence quarks at high x is not only of theoretical interest, it is also important for the search for new physics features. In particular, jets with very large transverse energy (E_T) with respect to the beam direction at the Tevatron are dominantly produced by quark interactions and small differences in the quark distributions can induce large effects on the extracted gluon density.

At high x, the u quark distribution is well constrained by DIS on protons (in particular the fixed target experiments NMC and BCDMS), but the d quark distribution is extracted from deuterium data, where Fermi motion and nuclear binding have to be taken into account, leading to large uncertainties.

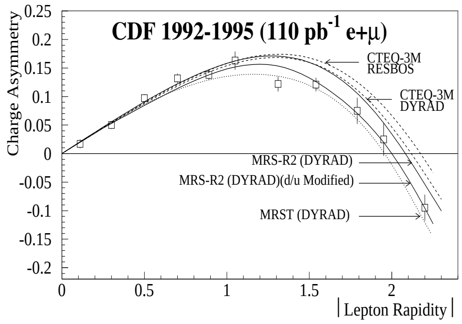

Figure 7. Rapidity distribution of the charged lepton in W leptonic decay, measured by the CDF collaboration at the Tevatron [17]. The effect of the modification of the d/u ratio limit [16] is shown by the difference between the MRS-R2 predictions; the MRST pdf's include the present measurement.

A recent reanalysis of NMC and SLAC data [16] favours a ratio $d/u \ \rightarrow \ 0.2$ for $x \ \rightarrow \ 1$, instead of the limit 0 which is usually chosen, albeit without strong theoretical motivation. This reanalysis appears to improve the description of ν-Fe cross section, of jet E_T distributions at the Tevatron, of e^+p CC interactions at HERA (although, in view of the large experimental errors, global fits of parton distributions show little sensitivity to this modification of the d/u ratio limit - see Fig. 6) and of the $W \rightarrow l\nu$ charge asymmetry (Fig. 7).

A significant improvement of the knowledge of the d distribution will be obtained from e^+p CC interactions at HERA, where no nuclear binding effects are present, after the accelerator upgrade of year 2000 which will result in an increase by a factor 15 of the presently accumulated luminosity.

3.1.2. The gluon density. The main reactions relevant for the measurement of the gluon momentum distribution $xG(x)$ for $x > 0.1$ are high E_T jet (Fig. 8a) and prompt photon production (Fig. 8b) in $p(\bar{p})p$ interactions. Unfortunately, both suffer of severe problems.

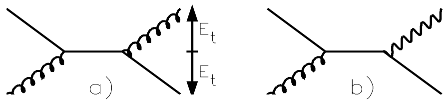

Figure 8. Two processes testing the gluon content of the proton in $p(\bar{p})p$ interactions: a) high E_T jet production ; b) prompt photon production.

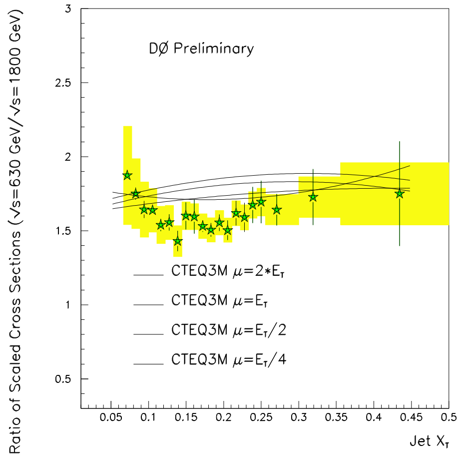

Figure 9. Ratio of scaled cross section for D0 jet production at $\sqrt{s} \ = \ 630$ GeV and $\sqrt{s} \ = \ 1800$ GeV, as a function of $x_T \ = \ 2E_T/\sqrt{s}$ [18]. The shaded area corresponds to the systematic uncertainties. The lines correspond to NLO calculations for different values of the QCD scale μ.

High E_T jet production has been a much debated question [6]. It now appears that D0 and CDF results are compatible within systematic errors (including normalisation uncertainties). However, the D0 jet analysis reveals an inconsistency between the ratio of the measurements at $\sqrt{s} = 630$ GeV and $\sqrt{s} = 1800$ GeV and that of the corresponding NLO calculations (Fig. 9). It is unclear whether this is an experimental problem or if it is due to a large influence of NNLO corrections resulting in an effective change of scale. In addition, the extraction of the gluon distribution from high E_T jet measurements is affected by the uncertainty of the d/u ratio at large x. In summary, the uncertainty on the gluon distribution extracted from large E_T jets has not significantly decreased recently.

Prompt photon production is another process directly testing the gluon content of the proton, but complications arise from the need to resum soft gluon emission, leading to a modification of the NLO predictions. This is parameterised in the form of an

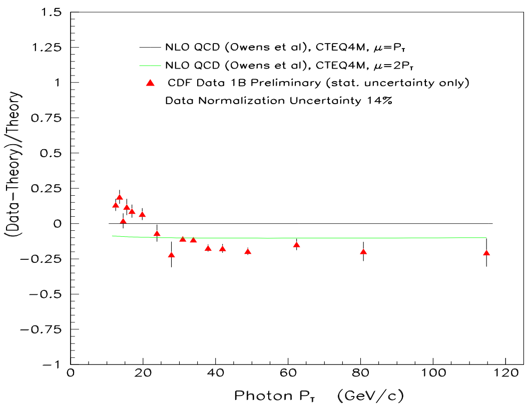

Figure 10. CDF measurement of the p_T distribution of prompt photons in $p\bar{p}$ interactions, compared to the predictions of the CTEQ4M pdf's for two different values of the QCD scale μ [20].

intrinsic k_T contribution to the gluon distribution, with $\langle k_T \rangle \simeq 1.2$ GeV for high energy fixed target data (prompt photon and $\mu\mu$, $\gamma\gamma$, π^o and jet data from the E706 experiment [19]). At the Tevatron collider, an intrinsic $\langle k_T \rangle \simeq 3.5$ GeV is required to describe the prompt photon measurement by CDF [20] (Fig. 10).

Because of these large NNLO corrections, which seem not to be well under control, prompt photon data are not used by the CTEQ group [8], and the gluon density is extracted from large E_T jet data. Conversely, the choice of the MRST group [9] is to use WA70 prompt photon data, with a spread of values of $\langle k_T \rangle$, and not to use the jet data. In this case, different choices of $\langle k_T \rangle$ lead to significant differences for the absolute dijet rate predictions, but not for the shape of the distributions.

In conclusion, gluon parameterisations can largely differ for $x > 0.1$ (see Fig. 11). With increasing Q^2, the gluon density at large x rapidly decreases, but the discrepancies remain important, which has some influence for $0.01 < x < 0.1$ because of the constraint imposed by momentum sum rules.

3.1.3. The $\bar{d}/\bar{u}$ sea for $0.02 < x < 0.3$. The Gottfried sum rule [22], related to quark counting, states that

$$\int_0^1 dx/x\,[F_2^p(x) - F_2^n(x)] = 1/3$$

if $\bar{u}(x) = \bar{d}(x)$. This is expected in perturbative QCD (pQCD), in view of the equal coupling of the gluons to $u\bar{u}$ and $d\bar{d}$ pairs.

The NMC [23] and NA51 [24] experiments have reported a breaking of this hypothesis, respectively for $\int(\bar{d}-\bar{u})\,dx$ (at $Q^2 = 4\,\mathrm{GeV}^2$) and for $x = 0.18$. At this

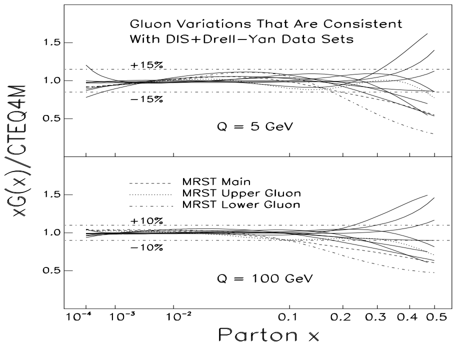

Figure 11. Various choices of the CTEQ5 and MRST gluon momentum distributions, normalised to the CTEQ4M parameterisation [21].

conference, the E866 collaboration has reported final results from Drell-Yan proton nucleon scattering [25], showing that the $\bar{d}$ and $\bar{u}$ distributions differ for $0.02 < x < 0.3$ (see Fig. 12). This is confirmed by the HERMES experiment studying charged pion production in ep and en scattering, assuming isospin symmetry [26].

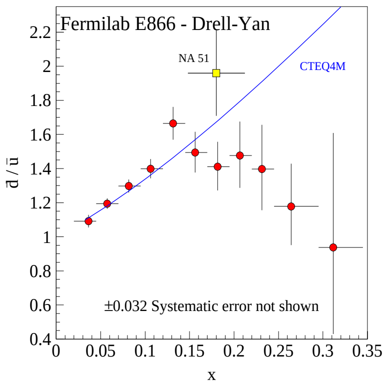

Figure 12. The ratio $\bar{d}/\bar{u}$ in the proton as a function of x measured by the E866 experiment [25], compared to the CTEQ4M pdf prediction, which used the NA51 data point [24].

The $\bar{d}/\bar{u}$ asymmetry is non-perturbative in origin. Only a small fraction of the effect is due to Pauli blocking, the main contribution being attributed to an asymmetry in the pion clouds accompanying the nucleons [27].

3.2. Parton distributions and QCD.

3.2.1. Structure functions and scaling violations. As shown in Fig. 13, the DGLAP QCD evolution describes ep DIS data at HERA with an impressive precision for $2 \cdot 10^{-5} < x < 0.65$ and $1 < Q^2 < 3 \cdot 10^4$

GeV^2 [28, 29]. No need is found for higher twist or other non-DGLAP effects.

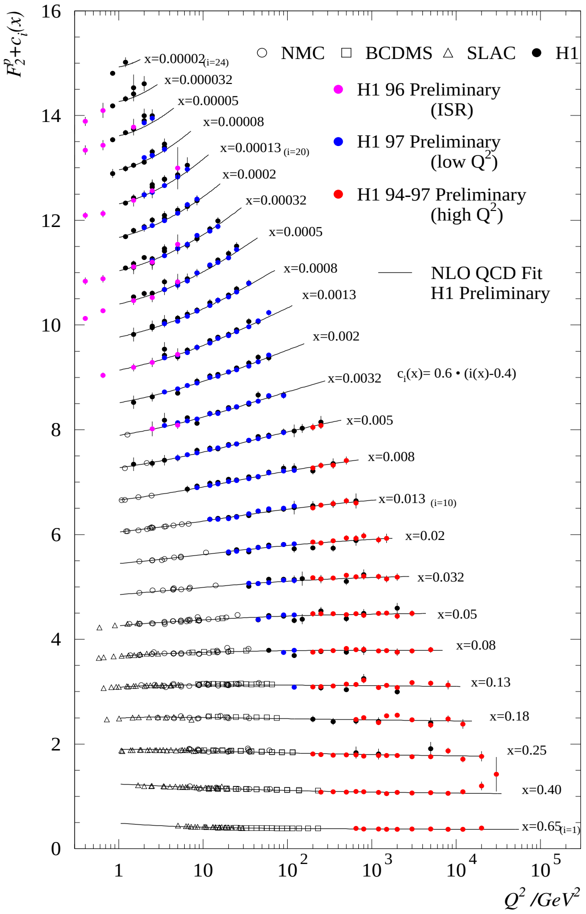

Figure 13. Measurements of the F_2 structure function by the H1 and fixed target collaborations; the lines are results of a global NLO QCD fit.

In most of this wide kinematic domain, the u and d quark densities in the nucleon are thus precisely known. The gluon density distribution is not directly tested, but is extracted from scaling violations with a good precision (see Fig. 14). It is successfully tested in several processes, in particular jet and charm production.

3.2.2. Gluons and jets. In DIS, high E_T jets are mainly due to the photon gluon fusion process (Fig.15a), with a smaller contribution from the QCD-Compton mechanism (Fig.15b).

The differential distributions for dijet production measured by H1 and ZEUS are in agreement [30, 31] with predictions using the gluon momentum distribution extracted from scaling violations, for $0.005 < \xi < 0.3$ and $Q^2 > p_T^2$ †. Here, ξ is the fraction of the proton momentum carried by the gluon entering the hard interaction: $\xi = x\ (1 + M_{jj}^2/Q^2)$, where M_{jj} is the two-jet invariant mass and x the Bjorken scaling variable. The measurement of the production rate allows a precision extraction of α_s.

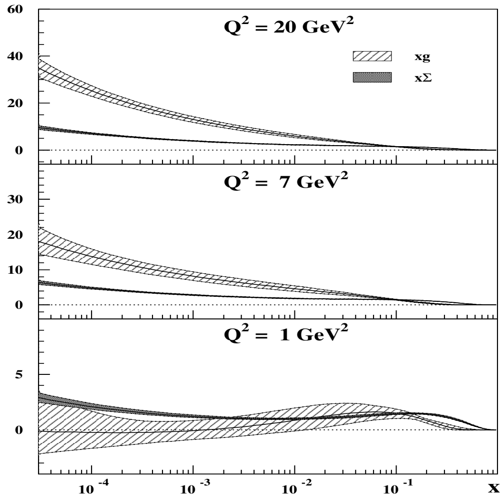

Figure 14. The gluon $xG(x)$ and the quark singlet $x\Sigma(x)$ momentum distributions plotted as a function of x for several values of Q^2, obtained from a NLO QCD fit to the ZEUS e^+p cross section measurement [12].

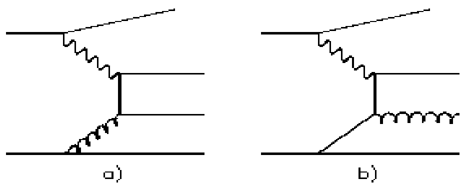

Figure 15. High E_T jet production in DIS: a) photon gluon fusion; b) the QCD-Compton mechanism.

Conversely, using the α_s measurement taken from other processes, a joint fit to the Q^2 evolution of F_2 (which fixes the quark densities) and to the dijet rate (which drives the gluon density) can be performed. The gluon density extracted from the dijet production [30] is in agreement with that obtained from scaling violations alone (see Fig. 16).

3.2.3. Gluons and charm. Charm production is also directly related to the gluon density, since charm quarks are radiatively produced through the photon gluon fusion process (see Fig. 17). The charm contribution to the DIS cross section, expressed in the form of a

[3] For $Q^2 < p_T^2$, a resolved photon component may also have to be taken into account [32].

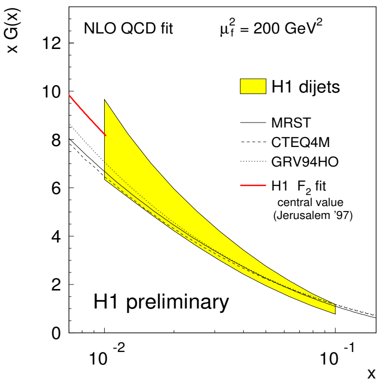

Figure 16. Gluon momentum distribution extracted by H1 from dijet production (shaded area) [30], compared to standard pdf's and to the distribution obtained by H1 from a DGLAP fit to the inclusive cross section measurement [11].

"charm structure function" F_2^c, is studied through the decay chain $D^* \to D^\circ \pi$; $D^\circ \to K\pi$ or $K3\pi$ [33, 34].

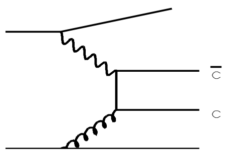

Figure 17. Charm production in DIS (photon gluon fusion process).

The fast increase of F_2^c with decreasing x (see Fig. 18) confirms the gluonic origin of charm. This increase is faster than for F_2, and at low x (i.e. high energy W) and high Q^2, charm production accounts for some 25 % of the DIS cross section [33]. The charm measurements by H1 and ZEUS agree well with predictions based on gluon momentum distributions obtained from global fits to the F_2 scaling violations.

An interesting feature of a measurement of the gluon density obtained from charm production (Fig. 19) is that it does not depend on a form assumed *a priori* for $xG(x)$. However the charm measurement suffers of rather large systematic errors since models are needed to correct for experimental cuts and extract the full D^* rate from the observed signal, and to relate the D^* distributions to the charm quark distribution (effects of the charm quark fragmentation and of final state interactions between charm quarks and proton remnant, leading to a beam drag). Uncertainties also arise from the choice of the value of m_c.

3.2.4. Determination of F_L. Following relation (1), the differential NC cross section is proportional (for $Q^2 \ll m_Z^2$) to the reduced cross section $\sigma_r = F_2(x, Q^2) - y^2/Y_+ \, F_L(x, Q^2)$. Two consistent determinations of the longitudinal structure function F_L have been obtained by H1 at large y [35] (Fig. 20):

- the QCD evolution of the pdf's is assumed to be valid at large y, and F_L is computed by the subtraction of the F_2 contribution from σ_r;
- a linear extrapolation of the derivative $\partial F_2/\partial \log y$ is assumed for large y, providing a determination of F_L.

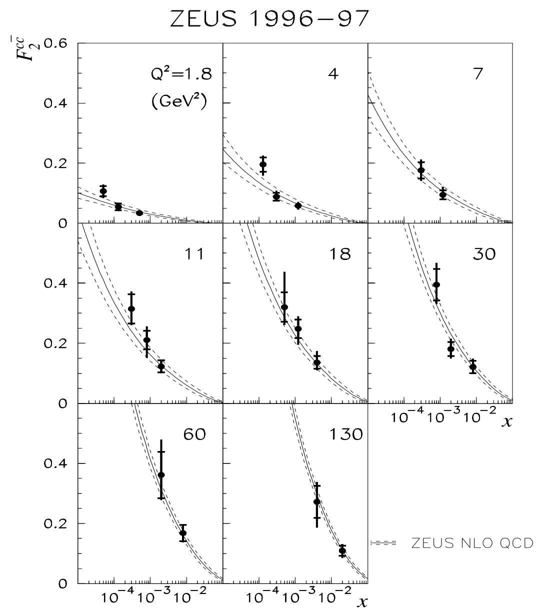

Figure 18. Charm structure function F_2^c measured by ZEUS as a function of x for several values of Q^2 [33]. The curves correspond to a NLO calculation using the pdf's extracted by ZEUS from a QCD fit to the inclusive DIS measurement [12].

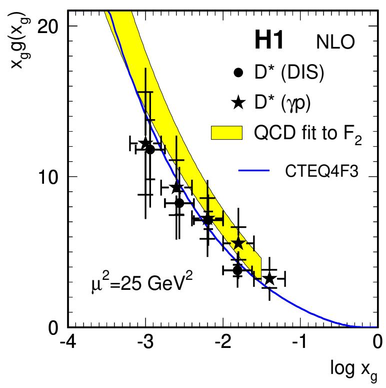

Figure 19. Gluon momentum distribution obtained by H1 from measurements of charm production [34]. The shaded area corresponds to a NLO QCD fit to the inclusive DIS measurement [11]. The curve represents the CTEQ4F3 parameterisation.

These determinations are consistent with QCD predictions, which are driven by the gluon distribution in the proton.

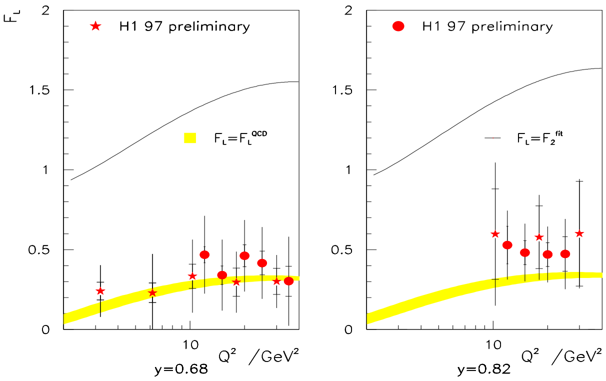

Figure 20. F_L determination by H1 for two values of y, using the subtraction method (dots) and the derivative method (stars) [35]. The grey areas represent the QCD predictions; the lines represent the case where $F_L = F_2$.

3.3. Conclusion.

In conclusion, the proton structure function $F_2(x,Q^2)$ is measured over a huge kinematic domain, and QCD fits describe the scaling violations with high precision. Except for uncertainties at high x for the d/u ratio and for the gluon density, the parton distributions are thus precisely known. In particular, the gluon density extracted from fits to the scaling violations in the intermediate x domain is in good agreement with measurements of dijet and charm production and with determinations of F_L.

4. Low x physics.

In DIS, parton emission (mainly gluons) between the struck quark and the target remnant can be described for two limits, calculable in pQCD (see Fig. 21):

- the high virtuality limit (large Q^2), described by the DGLAP evolution equations [13] which correspond to a strong ordering in k_T of the emitted gluons (from $k_T^2 \simeq Q^2$ at the photon vertex to $k_T^2 \simeq 0$ at the target vertex), with resummation of the $[\alpha_s \log Q^2]^n$ terms (LO). In this limit, k_T is thus small for a large x gluon.
- the high energy limit (small x, with $W^2 \simeq Q^2/x$), described by the BFKL equations [36] which correspond to a strong ordering in $1/x$ (from very small x to $x \simeq 1$), with resummation of the $[\alpha_s \log 1/x]^n$ terms. In this case, there is no k_T ordering and k_T can be large even for a large x gluon.

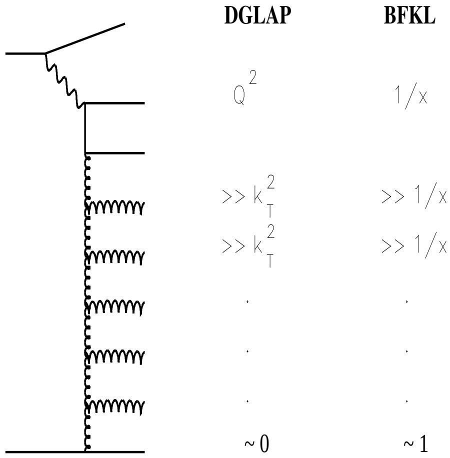

Figure 21. Two limiting cases of QCD evolution in DIS: high virtuality (DGLAP evolution) and high energy (BFKL evolution).

A striking prediction of the BFKL evolution at LO is a strong energy dependence of the cross section: $\sigma(s) \propto s^{\alpha_{BFKL}-1} \simeq s^{0.4-0.5}$, whereas in "soft" hadron–hadron interactions [38], only a weak energy dependence of the cross section is observed: $\sigma(s) \propto s^{0.08-0.10}$ (here, s is the square of the total hadronic energy, denoted by W in DIS) †.

The most important result at HERA is probably the observation of a fast increase of the F_2 structure function at low x in the DIS regime (see Fig. 22), attributed to the increase of the gluon density. This is parameterised for $x < 0.1$ in the form $F_2(x,Q^2) \propto x^{-\lambda}$ (Fig. 23). Whereas at small Q^2 λ is low and close to the "soft" value 0.08-0.10 [12, 35] the high value of λ measured at high Q^2 may be consistent with a BFKL interpretation of the x evolution of the structure function (remember that $1/x \propto W^2$). However, this behaviour is also compatible with a DGLAP-type evolution, as demonstrated by the quality of the DGLAP fits to the Q^2 evolution in Figs. 13 and 22 †.

The relevance of the BFKL approach can thus not be demonstrated on the basis of the total cross section

[4] First studies of NLO contributions [37] indicated that the corresponding corrections can be very large, suggesting an unstable behaviour of the calculation. Recently, higher order corrections were found to be better under control when using more "physical" renormalisation schemes than the $\overline{MS}$ scheme [39, 40].

[5] Note that the freedom of choice of the pdf parameterisations at the starting value of the DGLAP evolution may "hide" BFKL features. Note also that gluon emissions ("rungs" of the BFKL ladder) are separated by about two units in rapidity, implying that only a small number of "rungs" plays a role at HERA energies. The rapidity of a particle is given with respect to a given axis z as $y = \frac{1}{2}\log\frac{E+p_z}{E-p_z}$; the rapidity interval between two particles is invariant under a boost along z.

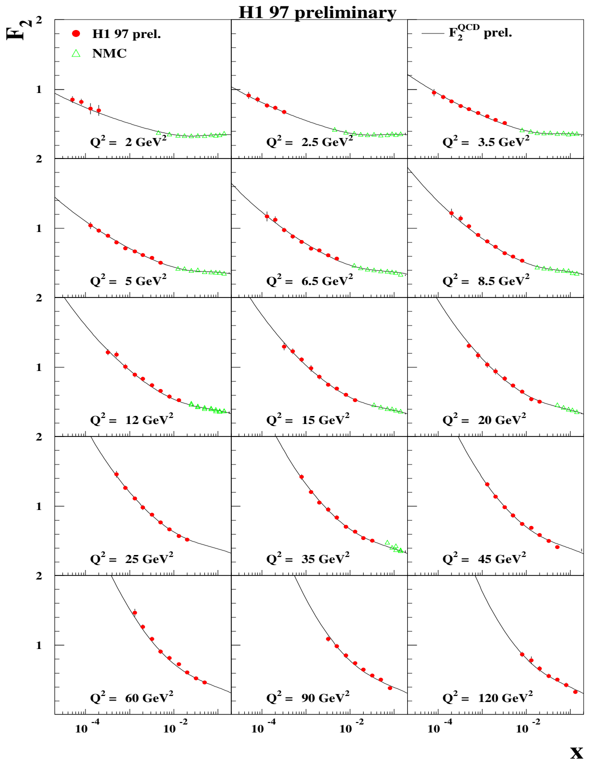

Figure 22. Measurement of the $F_2(x, Q^2)$ structure function by the H1, NMC and BCDMS collaborations as a function of x in bins of Q^2 [35]. The lines show the result of a NLO DGLAP fit.

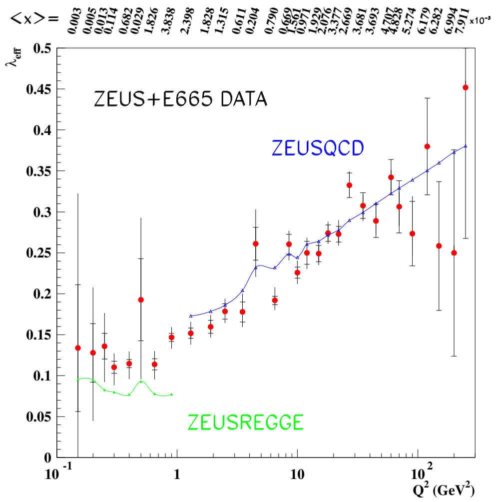

Figure 23. ZEUS measurement of the parameter $\lambda = \mathrm{d}\ln F_2/\mathrm{d}\ln(1/x)$ describing, for fixed Q^2, the rise of F_2 towards low x [12]. The lines represent the ZEUS NLO DGLAP fit for $Q^2 > 1\ \mathrm{GeV}^2$ and a Regge type parameterisation for $Q^2 < 1\ \mathrm{GeV}^2$.

measurements alone. Footprints for BFKL evolution are to be searched for specifically in exclusive channels, in particular those characterised by both a strong energy evolution and the absence of a strong k_T ordering. In a high energy (very low x) DIS process, a marked difference characterises the emission of partons carrying a large fraction of the proton momentum: for BFKL, such partons can be emitted with a large k_T, whereas for DGLAP they are restricted to small k_T values.

4.1. *Large energy, large p_T π° production at HERA.*

The process $e^+p \to e^+\pi^\circ X$ has been studied by H1 [41] for DIS events with large π° energy and large $p_T^{\pi^\circ}$ (defined with respect to the $\gamma^* p$ axis): $x_{\pi^\circ} = p_{\pi^\circ}/p_p > 0.01$, $p_T^{\pi^\circ} > 2.5$ GeV, for events with $Q^2 > 2$ GeV^2 and $5 \cdot 10^{-5} < x < 5 \cdot 10^{-3}$. For such events, the photon virtuality Q^2 and the transverse momentum squared of the parton emitted in the parton cascade, k_t^2, are thus of similar magnitudes. The π° meson is emitted close to the proton direction ("forward" direction), and is well separated in rapidity from the quark jet (see Fig. 24) †.

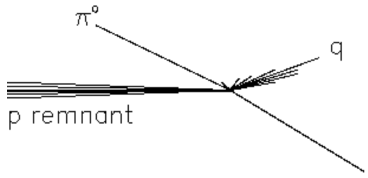

Figure 24. Final state topology for large energy, large p_T π° emission in DIS.

As shown in Fig. 25, the absolute cross section and the production rate for these events are consistent with predictions of a (modified) LO BFKL model [43] for several intervals in Q^2. They are not compatible with the predictions of the LEPTO6.5 model [44], which is based on the DGLAP evolution. A model [45] which includes a resolved photon contribution in DIS [32] gives a better, but not satisfactory description of the data.

4.2. *Dijets with a large rapidity separation at the Tevatron.*

The production, e.g. in $p\bar{p}$ interactions, of two high E_T jets separated by a large gap $\Delta\eta$ in (pseudo-)rapidity † (see Fig. 26) can also typically be described in a BFKL approach [46]: the larger the gap in rapidity, the larger the number of "rungs" (gluon emissions) in the BFKL ladder.

[6] A related process is the emission of a "forward" jet [42]. However the acceptance in the forward direction for jet reconstruction is reduced compared to that for detecting a π° meson.

[7] The pseudorapidity is given by $\eta = -\ln\tan(\theta/2)$; it corresponds with the rapidity in the limit of vanishing mass.

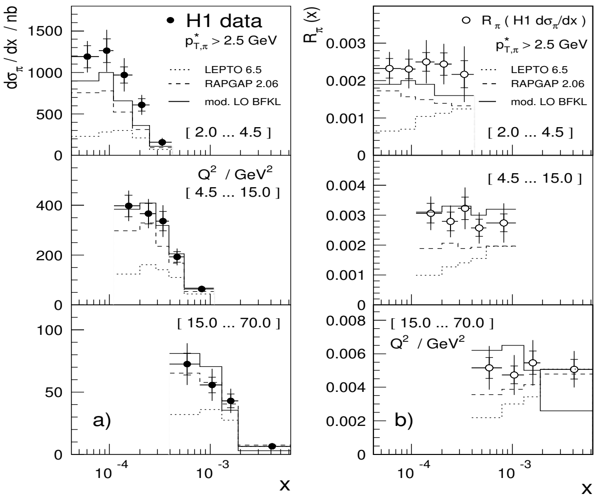

Figure 25. H1 measurement of π° production with $p_{\pi^\circ}/p_p > 0.01$, $p_T^{\pi^\circ} > 2.5$ GeV, as a function of x in 3 intervals of Q^2 [41]: left) cross section; right) production rate in DIS. The full histograms represent the predictions of the (modified) LO BFKL model [43]; the dotted histograms are the predictions of the LEPTO6.5 model [44]; the dashed histograms correspond to a model which includes a resolved photon contribution in DIS [45].

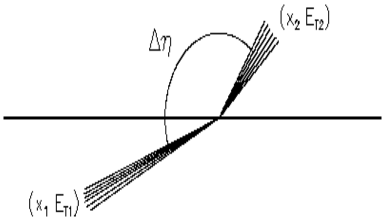

Figure 26. Two jets (x_1, E_{T1}) and (x_2, E_{T2}), separated by a large pseudorapidity gap $\Delta\eta$.

The cross section for this process is given following the BFKL evolution for jets of transverse energies E_1^T, E_2^T by the relation:

$$\sigma(x_1, x_2, Q^2, \Delta\eta) \propto x_1 P(x_1, Q^2)\ x_2 P(x_2, Q^2) \frac{1}{Q^2} \frac{e^{(\alpha_{BFKL}-1)\ \Delta\eta}}{\sqrt{\alpha_s\ \Delta\eta}}, \qquad (3)$$

where x_1 and x_2 are, respectively, the fractions of the beam particle energies carried by the partons entering the strong interaction, $xP(x, Q^2)$ being the (colour weighted) sum of the gluon and quark distribution functions, and $Q^2 \simeq E_1^T \cdot E_2^T$.

In relation (3), the test of the BFKL evolution is provided by the $\Delta\eta$ dependence of the cross section. At a given beam energy, varying $\Delta\eta$ means changing x_1 and x_2, which leads to uncertainties due to the pdf's. For this reason, the measurement was performed by the D0 collaboration [47] for jets with $E_T > 20$ GeV, for two different beam energies (with $\sqrt{s} = 630$ and 1800 GeV, respectively) but for fixed values of x_1, x_2 and Q^2, and thus different values of $\Delta\eta$. The ratio R of the two cross sections is given by $R_{1800/630} = e^{[\alpha_{BFKL}-1][\Delta\eta_{1800}-\Delta\eta_{630}]}\ /\ [\Delta\eta_{1800}/\Delta\eta_{630}]^{1/2}$.

The D0 measurements gives the value $R_{1800/630} = 2.9 \pm 0.3$ (stat.) ± 0.3 (syst.) for $\langle\Delta\eta_{630}\rangle = 2.6$ and $\langle\Delta\eta_{1800}\rangle = 4.7$. This value is incompatible with a QCD LO evolution, which asymptotically tends to 1 as $\Delta\eta$ increases. It is suggestive of a BFKL evolution but the present measurement would correspond to the high value $\alpha_{BFKL} = 1.7 \pm 0.1 \pm 0.1$.

4.3. Conclusion.

In summary, considerable theoretical work is providing increasingly reliable and stable higher order calculations of the BFKL evolution. On the experimental side, measurements of processes characterised by large rapidity separations between partons suggest the presence of BFKL processes. However Monte Carlo simulations including higher order contributions and details of hadron fragmentation are necessary in order to provide conclusive tests of BFKL predictions.

5. Diffraction.

5.1. Introduction.

Understanding diffractive interactions is of fundamental importance for the understanding of elementary particle physics since diffraction governs the high energy behaviour of elastic cross sections and thus of total cross sections (this relation is provided by the optical theorem, which derives from the unitarity of the S-matrix).

Moreover, the hypothesis of analyticity of the S-matrix and the crossing property of elementary particle processes allow relating the physical amplitudes in the s- and t-channels. In particular, the energy dependence of total cross sections in the s-channel is related to the properties (quantum numbers) of the particle states which can be exchanged for elastic scattering in the t-channel.

In the framework of Regge theory [48], the concept of exchange of particles in the t channel is extended to the exchange of "trajectories", defined in the squared four-momentum / angular momentum (t, α) plane. The mass squared and the spin of real particles with related quantum numbers are observed to define linear trajectories: $\alpha(t) = \alpha(0) + \alpha' \cdot t$. This linear behaviour prolongates in the negative t, virtual exchange domain. The energy dependence of cross sections is thus governed by the intercept α and the slope α' of the relevant trajectories.

For total cross sections, the optical theorem leads, when neglecting the real part of the elastic amplitudes, to the relation $\sigma_{tot} \propto s^{\alpha(0)-1}$. Among known particles, the ρ and f meson families ("reggeon" trajectory) have the highest intercept, with $\alpha_{I\!R}(0) \simeq 0.5$, implying that $\sigma \propto 1/\sqrt{s}$ for processes mediated by reggeon exchange; for the pion family, $\alpha_\pi(0) \simeq 0$ and $\sigma \propto 1/s$.

At high energy, the total hadron–hadron cross section is however known not to decrease, but to increase slightly with energy: $\sigma_{tot}^{hh} \propto s^{0.08-0.10}$ [38]. This behaviour is thus attributed to the exchange of an object which cannot be related to known hadrons and is found to carry the quantum numbers of the vacuum: the pomeron.

It is a challenge for QCD to provide a "microscopic" picture of the pomeron (see e.g. [49–52]). The simplest model is a two-gluon system, in contrast with reggeons and other mesons which are fundamentally two-quark systems (glueballs are thus possibly physical states related to the pomeron). Any QCD description of high energy scattering needs to account for the pomeron properties, in particular the increase of total cross sections with energy. The observed power-law for this increase is however incompatible at very high energy with bounds arising from the unitarity of the S-matrix (Froissart bound). It is thus a major task to understand how QCD offers a mechanism for the damping of the total cross section at high energy.

It should be stressed that alternative models aim at explaining diffraction by soft colour recombination of partons, without a reference to the concept of pomeron [44, 53].

5.2. Diffraction in DIS at HERA.

5.2.1. Diffractive structure function and energy dependence. The experimental study of the pomeron structure is facilitated by a process which generalises elastic scattering: diffractive dissociation $a + b \rightarrow X + b$, with $M_X \ll \sqrt{s}$, the (ab) cms energy – see Fig. 27 (in "double diffraction", both states a and b are excited into small mass systems). Diffractive dissociation is explained by the differential absorption by the target of the various hadronic states which build up the incoming state [54].

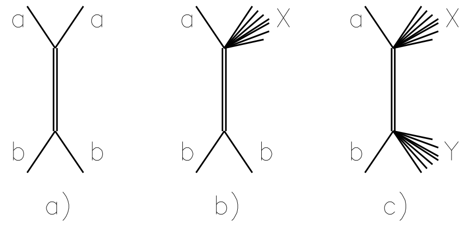

Figure 27. a) elastic scattering; b) single diffractive dissociation; c) double diffraction.

It was an important observation at HERA that 8 to 10 % of the DIS cross section is due to diffractive dissociation (Fig. 28). These events are characterised by a large gap in (pseudo-)rapidity $\Delta\eta$, devoid of hadronic energy, between the hadronic system X, of mass M_X, and the scattered proton (or the baryonic system Y resulting from proton excitation), implying the exchange of a colour singlet system. The gap is kinematically related to a small value of M_X, $M_X \ll W$; for small Q^2, the momentum fraction lost by the proton (or the excited system) is $x_L \simeq M_X^2/W^2 \ll 1$.

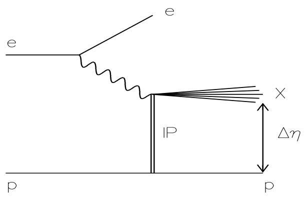

Figure 28. Diffractive dissociation at HERA.

A unique tool for testing the structure of the pomeron is thus provided at HERA by diffractive deep inelastic scattering (DDIS). Following the model of inclusive DIS, a "diffractive structure function" $F_2^{D(3)}(x_{I\!P}, \beta, Q^2)$ is extracted from the inclusive DDIS cross section [55–59], with $x_{I\!P} \simeq (Q^2 + M_X^2)/(Q^2 + W^2) \simeq 1 - x_L$, $\beta \simeq Q^2/(Q^2 + M_X^2)$ and $x = x_{I\!P} \cdot \beta$ †.

It has been proven in pQCD [61] that the amplitudes for DDIS processes factorise into a part which depends on $x_{I\!P}$ (a "pomeron flux factor"), and a "structure function" $\tilde{F}_2^D(\beta, Q^2)$ corresponding to a universal partonic structure of diffraction [62]. The variables $x_{I\!P}$ and β can thus be interpreted, respectively, as the fraction of the proton momentum carried by the pomeron, and the fraction of the pomeron momentum carried by the struck quark.

In a Regge approach, the "pomeron flux factor" follows a power law: $F_2^{D(3)}(x_{I\!P}, \beta, Q^2) \propto (1/x_{I\!P})^{2\alpha_{I\!P}-1} \cdot \tilde{F}_2^D(\beta, Q^2)$.

In photoproduction, HERA measurements [63, 64] give for the pomeron intercept values consistent with the "soft" value $1.08 - 1.10$. In DIS, the pomeron intercept $\alpha_{I\!P}(0)$ is significantly higher †: the H1 measurement [55] is $\alpha_{I\!P}(0) = 1.20 \pm$

[8] When diffractive events are selected by the presence of a gap in rapidity devoid of hadronic energy, the four-momentum squared t at the proton vertex is usually not measured, and the measurements are integrated over t. With the use of their proton spectrometer, the ZEUS experiment has performed a measurement of the t distribution [60].

[9] In the HERA energy range, pomeron exchange dominates rapidity gap events for $x_{I\!P} \lesssim 0.01$; for higher $x_{I\!P}$ values (lower energy), reggeon exchange has also to be taken into account (see e.g. [55]).

$0.02\,(\mathrm{stat.}) \pm 0.01\,(\mathrm{syst.}) \pm 0.03\,(\mathrm{model})$, and the ZEUS measurement [57] is $\alpha_{I\!P}(0) = 1.16 \pm 0.01\,(\mathrm{stat.})\ {}^{+0.04}_{-0.01}\,(\mathrm{syst.})$ ($\alpha_{I\!P}(0)$ has here been computed from the ZEUS measurement of $\alpha_{I\!P}(\bar{t})$ using $\alpha' = 0.25\ \mathrm{GeV}^{-2}$ and $|\bar{t}| = 1/7.1\ \mathrm{GeV}^2$ [60]).

At this conference, ZEUS has presented the measurement [58] $\alpha_{I\!P}(0) = 1.17 \pm 0.03\,(\mathrm{stat.})\ {}^{+0.04}_{-0.06}\,(\mathrm{syst.})$ in the range $0.22 < Q^2 < 0.70\ \mathrm{GeV}^2$ (Fig. 29). A transition from a soft to a hard behaviour thus happens at low Q^2 values. It should be noted that the value of $\alpha_{I\!P}(0)$ extracted from the diffractive cross section at low Q^2 is similar to that obtained from the total $\gamma^* p$ cross section in this domain (see Fig. 29). This means that the W dependence of the diffractive cross section is steeper than for the total cross section, as expected in Regge theory. In contrast, in the DIS domain at several GeV^2, the diffractive and total deep inelastic cross sections exhibit the same W dependence, at variance with Regge theory expectations. The value of $\alpha_{I\!P}(0)$ for diffractive scattering is thus lower than for the total cross section (the latter is represented on the figure by the curve labelled ALLM, which corresponds to a Regge motivated parameterisation of the total $\gamma^* p$ cross section [65]).

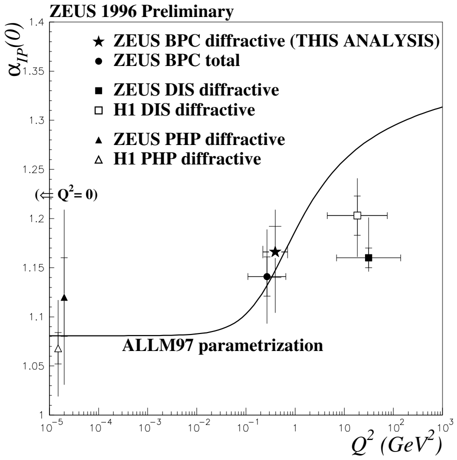

Figure 29. Measurements of $\alpha_{I\!P}(0)$ as a function of Q^2 [58]. The curve represents the total $\gamma^* p$ cross section, in the ALLM parameterisation [65].

5.2.2. Parton distributions. Parton distributions in the pomeron follow the DGLAP evolution equations, except for higher twist terms which can be significant, especially at large β values, $\beta \gtrsim 0.7 - 0.8$ [49, 51, 61].

Positive scaling violations are exhibited by DDIS at HERA, even for relatively large values of β (Fig. 30). QCD fits performed by H1 provide parton distributions

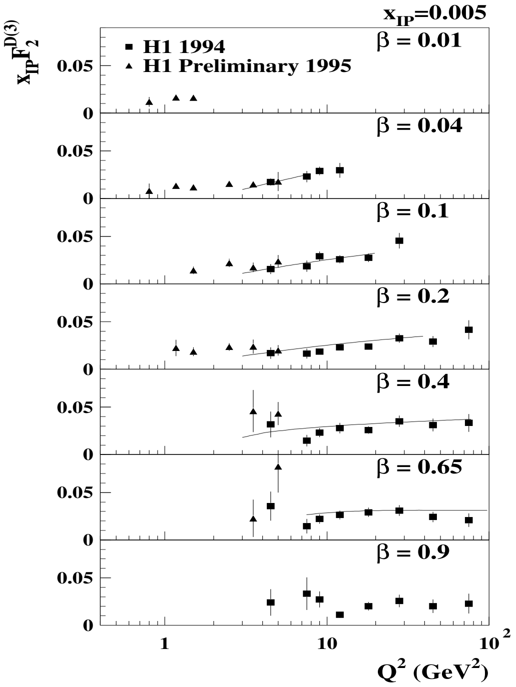

Figure 30. H1 measurement of the structure function $x_{I\!P} \cdot F_2^{D(3)}$ for $x_{I\!P} = 0.005$ as a function of Q^2 in bins of β [56]. The curves are the result of a DGLAP fit; they indicate the kinematical region over which the fit was performed.

in the pomeron which are dominated by (hard) gluons at the starting scale $Q_\circ^2 = 3\ \mathrm{GeV}^2$ [55] †.

The ZEUS collaboration [66] (and similarly the group [67]) has extracted the partonic content of the pomeron through a joint fit to the DDIS cross section, which probes the quarks directly, and diffractive jet photoproduction, which is mainly sensitive to the gluons. Although potentially sensitive to complications due to reinteractions between the diffracted proton and remnants of resolved photons (see below, section 5.3.2), these analyses confirm that most of the pomeron momentum is carried by gluons.

The pomeron pdf's extracted from QCD fits to inclusive DDIS can in turn be convoluted with scattering amplitudes to describe specific processes. This is performed using Monte Carlo simulations, in particular the Rapgap model [45]. Several analyses of hadronic final states show a good agreement between predictions and data [68, 69], which supports the universality of parton distributions in the pomeron.

The description of DDIS in terms of a partonic

[10] It should be stressed that only data up to $\beta = 0.65$ are used for the DGLAP QCD fits. The details of the pomeron structure at higher β values (e.g. the H1 "peaked" gluon or the H1 "flat" gluon distributions [55]) are thus extrapolations outside the measurement domain and should not be taken too literally.

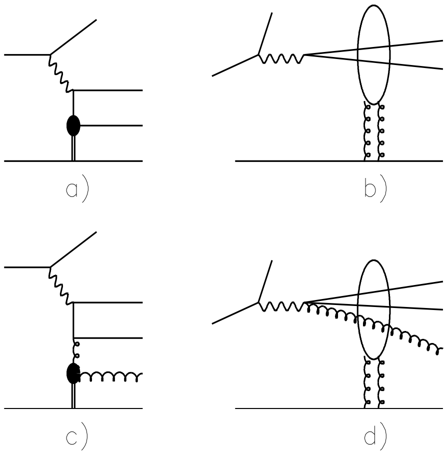

Figure 31. Deep inelastic diffractive scattering: left: the pomeron structure function approach (Breit frame): a) quarkonic pomeron, no pomeron remnant; c) gluonic pomeron, with a pomeron remnant; right: the photon Fock state approach (proton rest frame): b) $q\bar{q}$ Fock state; d) $q\bar{q}g$ Fock state; the pomeron is modelled as a two gluon system.

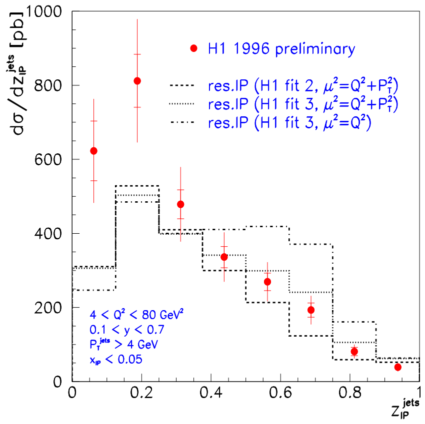

Figure 32. H1 measurement of the variable $z_{I\!P}$ for diffractive dijet production [72]. The histograms represent predictions of the Rapgap model [45] using pomeron pdf's extracted from inclusive DDIS: the dashed and dotted histograms are for a "flat" gluon, with two different QCD scales; the dashed-dotted histogram is for a "peaked" gluon [55].

structure of the pomeron (Breit frame approach) can be complemented by an approach using the proton rest frame (see Fig. 31). In this approach, the photon is described as a superposition of Fock states ($q\bar{q}$, $q\bar{q}g$, etc.), which are "frozen" during the hard interaction process [49–52].

At this conference, new results have been presented on two hard diffractive processes: dijet and charm production in DIS. Hard diffraction has also been studied at HERA in the case of dijet photoproduction [70, 71].

5.2.3. Diffractive dijet production. The H1 collaboration has measured diffractive dijet production with $p_T^{jet} > 4$ GeV (p_T is measured with respect to the $\gamma^* p$ axis), for DIS events with $4 < Q^2 < 80\ \mathrm{GeV}^2$ and $x_{I\!P} < 0.05$. A reasonable description of the differential distributions, both in normalisation and in shape, is obtained using pdf's extracted from inclusive DDIS [72].

Fig. 32 presents the distribution of the variable $z_{I\!P} = (M_{JJ}^2 + Q^2)/(M_X^2 + Q^2)$, where M_{JJ} is the invariant mass of the two jet system; $z_{I\!P}$ represents the fraction of the pomeron momentum carried by the partons (gluons) entering the hard process. In the absence of a pomeron remnant (Breit frame approach, Fig. 31a) or, equivalently, for a pure $q\bar{q}$ Fock state of the photon (rest frame approach, Fig. 31b), $M_{JJ} \simeq M_X$ and $z_{I\!P} \simeq 1$. This is observed only for a small fraction of the data, as expected as a consequence of "colour transparency": high p_T jets correspond to a small transverse distance between the quark and the antiquark, leading to mutual screening into a colour neutral object which is thus not detected by the proton (Fig. 31b). At variance, in the presence of an additional parton ($q\bar{q}g$ or higher order Fock states, Fig. 31d), the parton pair leading to the jets is not in a colour singlet state and the interaction with the proton takes place without attenuation due to colour transparency.

5.2.4. Diffractive charm production. Diffractive charm production in DIS has been studied both by the ZEUS and H1 collaborations in the channel $D^* \to K2\pi$, and by ZEUS for $D^* \to K4\pi$ [73, 74]. The diffractive charm production rate is measured by ZEUS to be $\simeq$ 8% of the total charm yield in DIS, and $\simeq$ 4% for H1. In view of the large errors, this corresponds only to a 2 σ discrepancy.

The shapes of the differential distributions are reproduced by calculations including the pomeron pdf's extracted from inclusive DDIS (see Fig. 33). As in the case of jet diffractive production, the absence of a peak close to 1 in the $z_{I\!P}$ distribution (not shown, H1 analysis [74]) is attributed to a dominant role of $q\bar{q}g$ or higher order Fock states, due to the effect of colour transparency.

5.2.5. Conclusions. The HERA experiments have provided a rich sample of results on diffractive processes in the presence of a hard scale (diffractive final state studies in DIS, jet and charm production). Within the limits of the present statistics, these data are consistent with the universality of the pdf's extracted from QCD fits to inclusive DDIS.

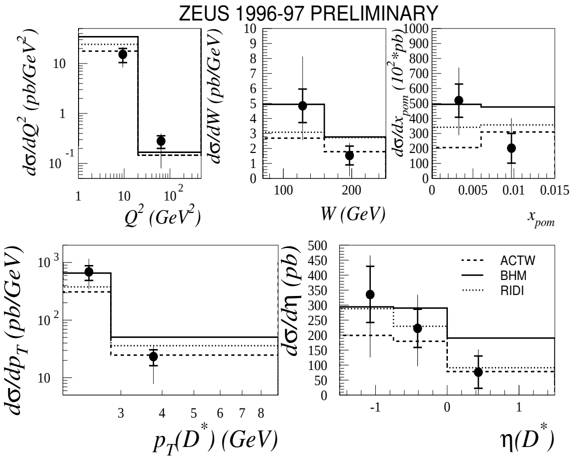

Figure 33. ZEUS measurement of the diffractive $D^* \to K4\pi$ cross section, as a function of Q^2, W, $x_{I\!P}$, the transverse momentum and the pseudorapidity of the D^* particle [73]. The histograms represent predictions of different models.

5.3. Hard diffraction at the Tevatron.

Even before HERA data taking, hard diffractive processes were observed at the CERN $p\bar{p}$ collider by the UA8 experiment [75]: while the diffractively scattered proton was detected in a proton spectrometer, high p_T jets were reconstructed in the central detector. This observation supported the hypothesis of a partonic component of diffraction [76].

At the Tevatron collider, hard diffraction is being extensively studied by the D0 and CDF collaborations [77], which complements the studies at HERA.

5.3.1. Single diffraction, double diffraction and double pomeron exchange. Hard single diffraction processes are studied at the Tevatron through the production of high p_T jets [78, 79] (Fig. 34a), and of W bosons [80], J/ψ mesons [81] and b particles [82] (Fig. 34b). These events are identified either through the detection of the diffractively scattered $\bar{p}$ in a proton spectrometer (CDF dijet events), or by the presence of a gap in pseudorapidity, devoid of hadronic activity, in the calorimeter and the tracking detector. Production rates are at the 1% level compared to the corresponding non-diffractive processes [83].

Hard double diffraction (see Fig. 35a) is studied through the production of two jets separated by a gap in rapidity attributed to colour singlet exchange [79, 84]. The rate of such events has been studied for $\sqrt{s} = 630$ and for $\sqrt{s} = 1800$. The ratio $R_{630/1800}$ is measured to be 2.4 ± 0.9 by CDF and 1.9 ± 0.2 by D0. This decrease of the diffractive process with increasing energy is at variance with expectations based on simple

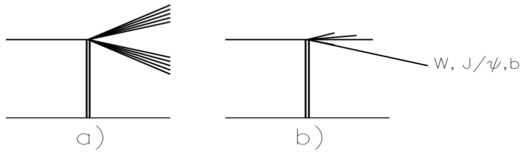

Figure 34. Hard single diffraction at the Tevatron: a) dijet production (gap/$\bar{p}$ + 2 jets); b) W, J/ψ, $b\bar{b}$ production.

BFKL evolution [85], but is predicted by models of soft colour recombination [53].

Finally hard dijet production has also been observed in the central detectors for events containing a scattered $\bar{p}$ identified in the proton spectrometer and a rapidity gap on the other side of the detector (CDF) [81], or a rapidity gap on each side of the detector (D0) [79] (Fig. 35b). These events are found to be produced at the 10^{-4} level of the corresponding non-diffractive process, which is consistent with a picture of double pomeron exchange, each pomeron exchange corresponding to a probability at the 1% level.

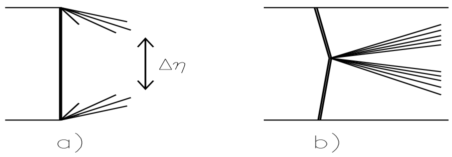

Figure 35. a) Dijet production with a gap in rapidity (jet + gap + jet), attributed to colour singlet exchange; b) dijet production by double pomeron exchange (gap/$\bar{p}$ + 2 jets + gap).

5.3.2. Factorisation breaking. Following a procedure similar to ZEUS [66], the CDF collaboration has determined the partonic content of the pomeron by taking advantage of the different sensitivities of the various processes (dijet, W and b production) to quarks and gluons [82]. The production rates were compared to predictions of the model Pompyt [86], which is based on the assumption of a factorisable pomeron flux; a hard partonic content of the pomeron was assumed.

A gluon fraction of 0.55 ± 0.15 is found, which is consistent with measurements at HERA (see Fig. 36), but the measured rates at the Tevatron are significantly lower than expected, the reduction factor being $D = 0.18 \pm 0.04$, whereas the order of magnitude of the HERA results is reproduced.

Similarly, predictions for the diffractive production rate of dijets and W bosons [67] and for charm production and double pomeron exchange [87] based on pomeron pdf's extracted from inclusive DDIS indicate that factorisation, which is verified in DIS, is broken in the case of diffractive hadron–hadron interactions.

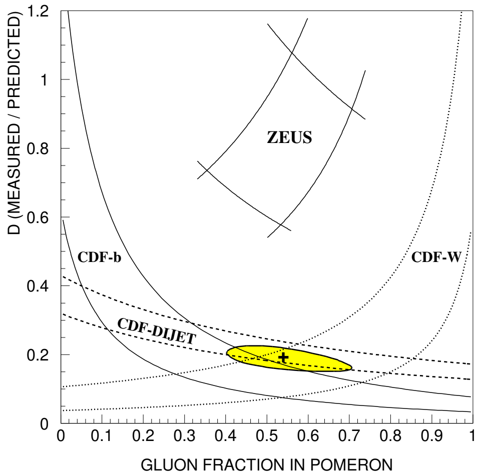

Figure 36. Ratio of measured to predicted diffractive rates as a function of the gluon content of the pomeron, for CDF dijet, W and b production and for a measurement by ZEUS of DDIS and diffractive jet photoproduction. The predictions are from the Pompyt model [86] with a hard pomeron structure. The shaded area is the 1 σ contour of a fit to the three CDF results [82].

The factorisation breaking is quantified in terms of a "survival probability". In hadron–hadron scattering, additional interactions between the diffractively scattered particle and remnants of the other beam particle can destroy the rapidity gap, whereas this effect is absent in DDIS [88]. This leads to a reduction of the diffractive rates at the Tevatron compared to predictions based on HERA DDIS data †. The energy dependence of the gap survival probability could also explain the observed decreasing rate of colour singlet exchange between jets for increasing $\sqrt{s}$.

5.3.3. Conclusion. In conclusion, active studies of hard diffraction are performed at the Tevatron, where diffractive processes represent about 1% of the corresponding non-diffractive processes. However, naive calculations for diffraction rates at the Tevatron based on pomeron pdf's obtained at HERA do not describe the data, which are about a factor 4 lower. This reduction of the gap survival probability could be attributed to underlying interactions between beam particle remnants.

5.4. Exclusive production of vector particles at HERA.

Numerous vigorous attempts are being made to use pQCD to calculate the cross section for several diffractive processes at HERA. Among them, diffractive (exclusive) production of a vector particle, either a photon or a vector meson, provides the most solid theoretical ground, as well as numerous high quality data. We concentrate here on the new results presented at this conference.

5.4.1. Deeply virtual Compton scattering. Deeply virtual Compton scattering (DVCS): $e + p \rightarrow e + p + \gamma$ (see Fig. 37a) is a gold-plated process for the study of pQCD in diffraction [89]. At high Q^2, the process is completely perturbatively calculable, since the incoming and outgoing photon wave functions and all couplings are known, and no strong interactions between final state particles affect the calculation.

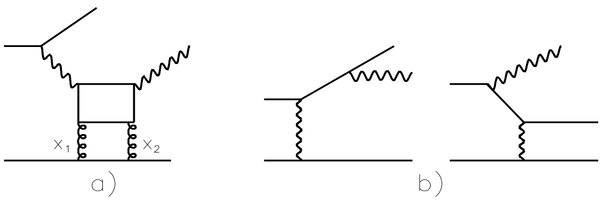

Figure 37. a) The DVCS process; b) the two LO diagrams contributing to the Bethe-Heitler (QED Compton) process.

To extract the DVCS cross section, account has to be taken of the interference with the Bethe-Heitler (QED Compton) process (Fig. 37b), but the two processes correspond to different regions of phase-space. The DVCS process is dominated by cases where the photon is emitted in the proton direction, since the photon flux factor in the electron is $\propto 1/y$, whereas for the Bethe-Heitler process, the photon is dominantly emitted in the electron direction.

The ZEUS collaboration [90] has for the first time at this conference shown evidence for the DVCS process, obtained with a sample of DIS events with $Q^2 > 6\ \mathrm{GeV}^2$ containing an electromagnetic cluster with energy larger than 10 GeV emitted in the backward region of the detector, a second electromagnetic cluster with energy larger than 2 GeV detected in the central region, at most one reconstructed track, and a maximum of 0.5 GeV additional energy reconstructed in the detector.

Fig. 38 shows the polar angle distribution of the second cluster, when identified as a photon The excess of events over the Bethe-Heitler prediction is consistent, in shape and normalisation, with the predictions of a simulation aimed at describing the DVCS and Bethe-Heitler processes, including the interference term.

It should be noted that, in the DVCS process, an incoming virtual photon is converted into a real photon. Kinematics imply that longitudinal momentum must be transferred to the proton, and the two gluons are thus not emitted and reabsorbed with the same energy ($x_1 \neq x_2$).

[11] In the case of diffractive photoproduction at HERA, additional interactions can also take place between the scattered proton and the resolved components of the photon. An indication for such an effect has been found in diffractive dijet photoproduction by H1 [71].

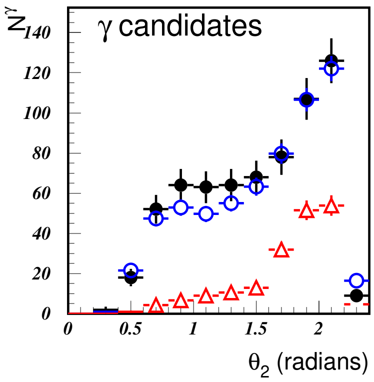

Figure 38. ZEUS measurement of the polar angle distribution of the photon candidate with energy larger than 2 GeV for $ep\gamma$ events [90]. The data are the full dots, the predictions for the Bethe-Heitler process are the open triangles, and the predictions of a DVCS + Bethe-Heitler simulation are the open circles.

This observation has led to the concept of "skewed parton distributions" [91]. The DVCS process is an ideal tool to study correlations between gluons in the proton.

5.4.2. Vector Meson Production. Vector meson (VM) production, both in photo- ($Q^2 \simeq 0$) and electroproduction has been intensively studied at HERA, for $\rho, \omega, \phi, \rho', J/\psi, \Psi', \Upsilon$ [92–98].

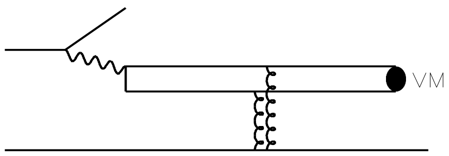

Figure 39. Vector meson production at high energy.

These processes can be computed as the convolution of three amplitudes involving very different time scales in the proton rest frame (see Fig. 39): the $\gamma \rightarrow q\bar{q}$ transition (a long distance process at high energy), the hard scattering of the $q\bar{q}$ pair (a short time process) and the $q\bar{q} \rightarrow VM$ recombination (on a typical hadronic scale of 1 GeV, boosted to the proton rest frame).

Energy dependence of the cross section. In the presence of a hard scale (large photon virtuality, heavy quark mass, large $|t|$), the hard process amplitude is modelled as two gluon exchange (reggeised gluons in a BFKL approach). The cross section is expected to be proportional to $|xG(x)|^2$ and thus exhibit a "hard" energy dependence, which is clearly observed in the case of J/ψ photoproduction (Fig. 40): the cross section can be parameterised, in a Regge inspired form, as $\sigma(\gamma^* p) \propto W^{4\alpha_{I\!P}(\bar{t})-4}$, with $\alpha_{I\!P}(\bar{t}) \simeq 1.20$, and QCD predictions [99] describe the data well. For light VM production (ρ, ϕ), $\alpha_{I\!P}(0)$ is observed to increase from a "soft" value typical of hadron–hadron scattering in photoproduction, to a value suggestive of a "hard" behaviour at high Q^2 (see e.g. [95]).

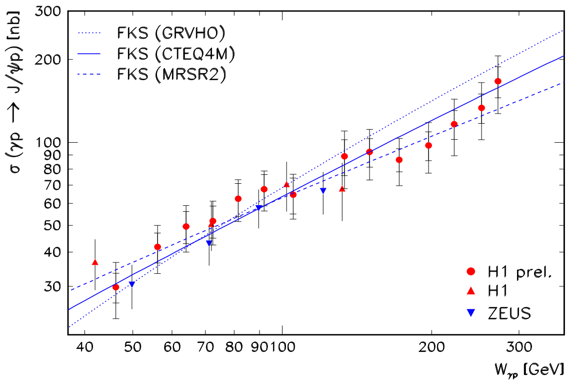

Figure 40. Energy dependence of the J/ψ photoproduction cross section at HERA [98], compared to QCD predictions [99] using several pdf's (the absolute normalisations have been adjusted to the data).

Q^2 dependence of the cross section. The Q^2 dependence of the cross section for electroproduction of ρ mesons can be parameterised in the form $\sigma(\gamma^* p) \propto 1/(Q^2+M_\rho^2)^n$, with $n = 2.3 \pm 0.1$ [95]. This behaviour is consistent with pQCD calculations ($\propto 1/Q^6$) [100], when account is taken of the Q^2 dependence of $xG(x)$ and α_s.

The ratio of cross sections for ϕ and J/ψ to ρ meson electroproduction [97] increases significantly with Q^2, towards values compatible with the quark counting rule (respectively the ratios 2/9 and 8/9), convoluted with the effects of wave functions [99]. It is interesting to note that, when plotted as a function of the variable $\frac{1}{4}(Q^2 + M_V^2)$, all $\gamma^* p \rightarrow VM\ p$ cross sections exhibit a common behaviour (see Fig. 41 [93]) †.

***t* dependence of the cross section.** The t dependence of the cross section for vector meson elastic production can be parameterised for low $|t|$ ($|t| \lesssim 1-2$ GeV^2) as $\mathrm{d}\sigma/\mathrm{d}t \propto e^{-b|t|}$, the slope parameter b being related to the transverse size of the interacting objects: $b \simeq R_p^2 + R_{VM}^2 + R_{I\!P}^2$. In Regge theory, the t distribution is expected to shrink with energy as $b(s) = b(s_\circ) + 2\alpha' \cdot \ln(s/s_\circ)$, with the trajectory slope $\alpha'_{I\!P} \simeq 0.25$ GeV^{-2}. At high energy, little shrinkage is expected in

[12] In the case of Υ production, large effects of skewed parton distributions may have to be taken into account [101].

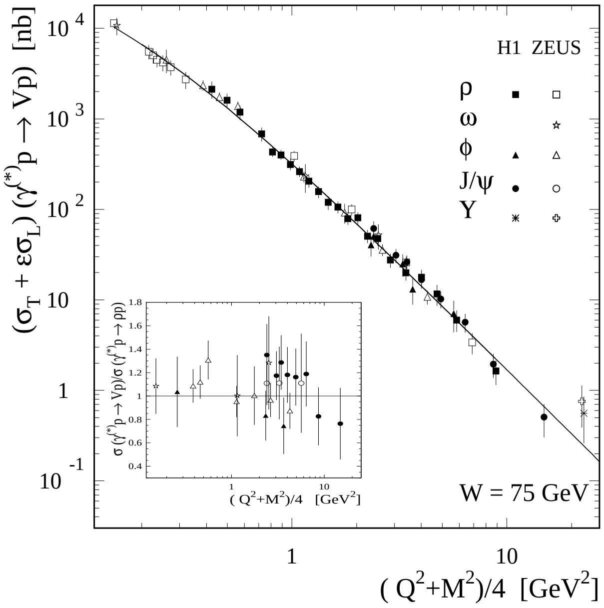

Figure 41. Cross section for elastic vector meson electroproduction, as a function of the variable $\frac{1}{4}(Q^2 + M_V^2)$ [93].

QCD (BFKL evolution), since α'_{BFKL} is expected to be small [39].

A measurement of the evolution of the t distribution as a function of W within one experiment, H1, has been presented for the first time at this conference for J/ψ photoproduction [98]. In spite of large errors, the slope of the trajectory $\alpha' = 0.05 \pm 0.15\ \mathrm{GeV}^{-2}$ is found to be consistent with 0 (Fig. 42), which supports the QCD expectation.

Polarisation. Detailed studies have been performed of the polarisations state of ρ [95,97] and ϕ [96] mesons, particularly in electroproduction. Although s-channel helicity conservation (SCHC) is dominantly observed to hold, a small but significant spin flip amplitude is measured in the transition from a transverse photon to a longitudinal ρ meson, at the level of $8 \pm 3\%$; the longitudinal to transverse transition and the double flip amplitude are compatible with 0 within errors [93]. These features are qualitatively reproduced by QCD based calculations [103].

The ratio $R = \sigma_L/\sigma_T$ of the longitudinal to the transverse cross section has been measured for ρ, ϕ and J/ψ meson production, and found to increase with Q^2 in the DIS region (Fig. 43). Although this increase is slower than anticipated [100], it is reproduced by some models based on QCD [103] or on generalised vector meson dominance (GVDM) [104]. When plotted as a function of the quantity Q^2/M^2 [93], the measurements

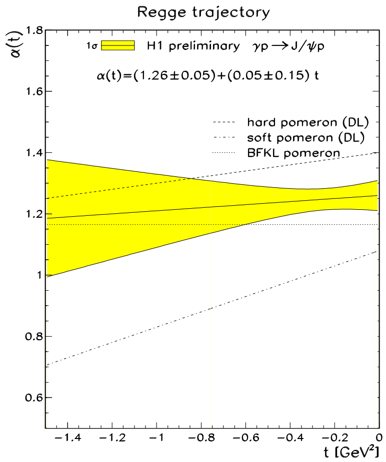

Figure 42. The Regge trajectory $\alpha(t) = \alpha(0) + \alpha' \cdot t$ measured by H1 for J/ψ photoproduction (full line, the error being given by the shaded area) [98]. The BFKL prediction [39] is shown as the dotted line, and the "soft" pomeron is the dashed-dotted line; the dashed line corresponds to a hard pomeron model [102].

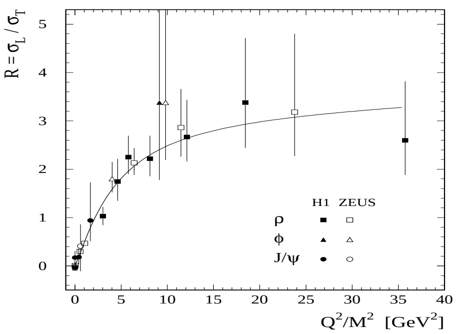

Figure 43. Ratio $R = \sigma_L/\sigma_T$ of the longitudinal to transverse cross sections for ρ, ϕ and J/ψ meson production, as a function of Q^2/M^2 [93]. The curve represents a phenomenological fit.

for the different vector mesons appear to follow a common behaviour (Fig. 43).

6. Indications for non-linear effects ?

The numerous results presented in this review provide a bright support for the presently available QCD calculations: impressive tests of the DGLAP evolution in DIS over a huge kinematic domain, indications for the relevance of the BFKL evolution in several channels at very high energy, relevance of the QCD approach for understanding diffraction and for exclusive vector particle production.

However, several intriguing features, both in inclusive DIS and in diffraction, suggest that this picture might have to be complexified. They are discussed in ref. [105–108], where it is advocated that they could be related to a very large density of partons at very low x and at Q^2 of the order of a few GeV^2, leading to saturation effects and a breakdown of the DGLAP and BFKL linear evolution equations. Unitarity constraints [107, 109] play an essential role in this dynamics.

In DIS, it is observed that the parton distributions extracted from (statistically satisfactory) DGLAP fits to the measured total cross section exhibit an unexpected behaviour at low Q^2: the gluon density at very low x becomes very small, even possibly negative, and the sea quark density is larger than for the gluon, whereas at larger Q^2 the gluon density drives the sea behaviour (see Fig. 14). In addition, the logarithmic derivative $\mathrm{d}F_2/\mathrm{d}\ln Q^2$ of the F_2 structure function, presented in Fig. 44 as a function of x and the corresponding average value of Q^2, shows an unexpected turn over at low x and $Q^2 \simeq$ a few GeV^2. Such a turn over is not observed at higher x for the same Q^2 range, suggesting that it is not due to higher twist effects.

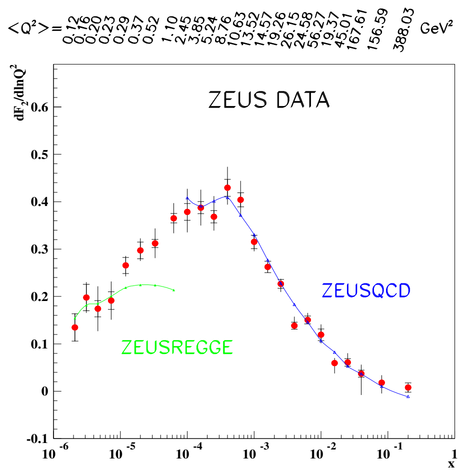

Figure 44. Logarithmic derivative of the F_2 structure function measured by ZEUS, as a function of x [12]; the corresponding average value of Q^2 is also indicated. The curves correspond to a NLO DGLAP fit and to a Regge parameterisation.

In diffractive DIS, the total cross section is observed to present a "hard" behaviour (see section 5.2.1 and Fig. 29), whereas the expectations are that the dominant topology would correspond to the "aligned jet model", with small p_T values and a "soft" energy dependence similar to that of hadron–hadron scattering. In soft hadronic diffractive dissociation $p(\bar{p}) + p \to p(\bar{p}) + X$, the measured cross section at high energy (CERN and Tevatron colliders) is significantly lower than expected from Regge theory (Fig. 45). Finally, as discussed in section 5.3.2, hard diffractive events at the Tevatron are suppressed compared to expectations based on inclusive DIS measurements. All these features are also attributed to very high parton densities and saturation effects.

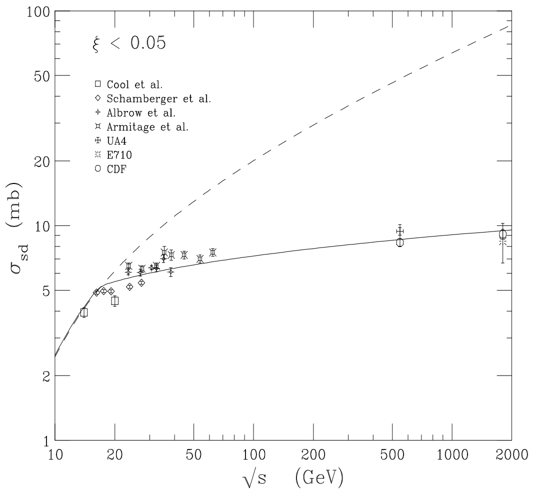

Figure 45. Total single diffraction cross section for $p(\bar{p}) + p \to p(\bar{p}) + X$ as a function of $\sqrt{s}$, compared to predictions from a Regge extrapolation of the low energy data (dashed line). The solid line describes a phenomenological model [110].

7. Conclusions.

In conclusion, huge amounts of data have been presented at this conference about hadron structure, low x physics and diffraction. The progress in these domains is impressive, both on the theoretical and the experimental sides. The parton distributions in the proton are precisely measured over most of the x domain, and new measurements are being performed. The ep total cross sections are described with high precision by the DGLAP evolution equations over a huge kinematic domain, but indications for the relevance of the BFKL evolution begin to appear in exclusive channels. A description of the pomeron in terms of partonic structure functions gives a consistent picture of the data in DIS at HERA, which is complemented by perturbative QCD calculations for hard processes. Hard diffraction is also intensively studied at the Tevatron in several channels. Finally, at HERA, the DVCS process and vector meson production, with a large amount of detailed data, provide a clean laboratory for a perturbative QCD understanding of diffraction. Intriguing features however suggest that the linear DGLAP and BFKL evolution equations might not be sufficient to describe all data, with possibly an indication for saturation effects at very low x and low Q^2 values.

Acknowledgements

I wish to thank numerous colleagues for their help in preparing this talk, in particular H. Abramowicz, K. Borras, B. Clerbaux, E.A. De Wolf, E. Elsen, M. Erdmann, A. Garfagnini, A. Goussiou, A. Martin, P. Merkel, C. Royon, S. Schlenstedt, U. Stoesslein, G. Snow. I also warmly thank B. Clerbaux for her useful comments to the text of these proceedings.

References

[1] E.A. De Wolf, these proc.
[2] A. Garfagnini (ZEUS Coll.), these proc.; D. Reyna (H1 Coll.), these proc.
[3] U. Stoesslein (HERMES Coll.), these proc; S. Rock (E155X Coll.), these proc.
[4] ZEUS Coll., papers 549, 550, 558, 559 subm. to this conf.; preprints DESY-99-56, DESY-99-59; P. Kooijman, these proc.
[5] H1 Coll., papers 157b, 157ai subm. to this conf.; preprint DESY-99-107; G. Bernardi, these proc.
[6] See M. Mangano, these proc.
[7] M. Glück, E. Reya, A. Vogt, *Eur. Phys. J.* **C6** (1998) 461.
[8] CTEQ Coll., H. Lai et al., *Phys. Rev.* **D55** (1997) 1280; hep-ph/9903282.
[9] A.D. Martin et al., *Eur. Phys. J.* **C4** (1998) 463; hep-ph/9907231.
[10] M. Botje, preprint NIKHEF-99-011.
[11] H1 Coll., S. Aid et al., *Nucl. Phys.* **B470** (1996) 3.
[12] ZEUS Coll., J. Breitweg et al., *Eur. Phys. J.* **C7** (1999) 609.
[13] V.N. Gribov, L.N. Lipatov, *Sov. J. Nucl. Phys.* **15** (1972) 438 and 675; Yu.L. Dokshitzer, *Sov. Phys. JEPT* **46** (1977) 641; G. Altarelli and G. Parisi, *Nucl. Phys.* **126** (1977) 297.
[14] M.A.G. Alvazis et al., *Phys. Rev.* **D50** (1994) 3102.
[15] R.S. Thorne, R.G. Roberts, *Phys. Lett.* **B421** (1998) 303; *Phys. Rev.* **D57** (1998) 6871.
[16] U.K. Yang, A. Bodek, *Phys. Rev. Lett.* **82** (1999) 2467.
[17] CDF Coll., F. Abe et al., *Phys. Rev. Lett.* **81** (1998) 5754.
[18] See e.g. V. Daniel Elvira (D0 Coll.), proc. of the 7th Int. Workshop on DIS and QCD, Zeuthen (1999).
[19] E706 Coll., L. Apanasevich et al., *Phys. Rev.* **D59** (1999) 74007.
[20] Paper 599 subm. to this conf.
[21] S. Kuhlmann, proc. of the 7th Int. Workshop on DIS and QCD, Zeuthen (1999).
[22] K. Gottfried, *Phys. Rev. Lett.* **18** (1967) 1174.
[23] NMC Coll., M. Arneodo et al., *Phys. Rev.* **D50** (1994) R1.
[24] NA51 Coll., A. Baldit et al., *Phys. Lett.* **B332** (1994) 244.
[25] E866 Coll., paper 602 subm. to this conf.; E.A. Hawker et al., *Phys. Rev. Lett.* **80** (1998) 3715; R. Towell, these proc.
[26] HERMES Coll., K. Ackerstaff et al., *Phys. Rev. Lett.* **81** (1998) 5519.
[27] See e.g. A. Szczurek et al., *Nucl. Phys.* **A596** (1996) 397.
[28] ref. [11]; H1 Coll., paper 157a subm. to this conf.; R. Wallny, these proc.
[29] ref. [12]; ZEUS Coll., papers 493, 553 subm. to this conf.; M. Wodarczyk, these proc.
[30] T. Carli, these proc.
[31] J. Terron, these proc.
[32] See experimental results in: H1 Coll., C. Adloff et al., *Phys. Lett.* **B415** (1997) 418; preprint DESY-98-205.
[33] ZEUS Coll., paper 523 subm. to this conf.; preprint DESY-99-101; L. Labarga, these proc.
[34] H1 Coll., papers 157g, 157p subm. to this conf.; preprint DESY-98-204; K. Daum, these proc.
[35] H1 Coll., paper 534 subm. to the 29th Int. conf. on HEP, Vancouver (1998).
[36] L.N. Lipatov, *Sov. J. Nucl. Phys.* **23** (1976) 338; E.A. Kuraev, L.N. Lipatov, V.S. Fadin, *Sov. Phys. JEPT* **45** (1977) 199; Y.Y. Balitsky, L.N. Lipatov, *Sov. J. Nucl. Phys.* **28** (1978) 822.
[37] V.S. Fadin, L.N. Lipatov, *Phys. Lett.* **B429** (1998) 127; G. Camici, M. Ciafolini, *Phys. Lett.* **B430** (1998) 349.
[38] A. Donnachie, P.V. Landshoff, *Phys. Lett.* **B296** (1992) 227; J. Cudell, K. Kang, S. Kim, *Phys. Lett.* **B395** (1997) 311.
[39] S.J. Brodsky et al., *JETP Lett.* **70** (1999) 155.
[40] See also contributions by M. Ciafolini, V. del Duca, V. Fadin, L. Lipatov, G. Salam, R.S. Thorne, proc. of the 7th Int. Workshop on DIS and QCD, Zeuthen (1999), and ref. therein.
[41] H1 Coll., paper 157g subm. to this conf.; preprint DESY-99-094.
[42] H1 Coll., S. Aid et al., *Phys. Lett.* **B356** (1995) 118; ZEUS Coll., J. Breitweg et al., *Eur. Phys. J.* **C6** (1999) 239.
[43] J. Kwiecinski, A.D. Martin, J.J. Outhwaite, hep-ph/9903439.
[44] G. Ingelman, A. Edin, J. Rathsman, Comp. Phys. Comm. **101** (1997) 108.
[45] H. Jung, Comp. Phys.Comm. **86** (1995) 147; see also http://www-h1.desy.de/ jung/rapgap.html.
[46] A.H. Mueller, H. Navelet, *Nucl. Phys.* **B282** (1987) 727.
[47] D0 Coll., paper 7li subm. to this conf.; A. Goussiou, these proc.

[48] P. Collins, *An Introduction to Regge Theory and High Energy Physics*, Cambridge Univ. Press, Cambridge (1977).
[49] N.N. Nikolaev, B.G. Zakharov, *Zeit. Phys.* **C64** (1994) 631.
[50] A. Bialas, R. Pechanski, C. Royon, *Phys. Rev.* **D57** (1998) 6899.
[51] J. Bartels et al., *Eur. Phys. J.* **C7** (1999) 443.
[52] A. Hebecker, these proc., and ref. therein.
[53] O.J.B. Eboli, E.M. Gregores, F. Halzen, hep-ph/9708283; hep-ph/9908374.
[54] M.L. Good and W.D. Walker, *Phys. Rev.* **120** (1960) 1857.
[55] H1 Coll., C. Adloff et al., *Zeit. Phys.* **C76** (1997) 613.
[56] H1 Coll., paper 571 subm. to the 29th Int. Conf. on HEP, Vancouver (1998).
[57] ZEUS Coll., J. Breitweg et al., *Eur. Phys. J.* **C6** (1999) 43.
[58] ZEUS Coll., paper 500 subm. to this conf.
[59] ZEUS Coll., paper 524 subm. to this conf.
[60] ZEUS Coll., paper 972 subm. to the 29th Int. Conf. on HEP, Vancouver (1998).
[61] J.C. Collins, *Phys. Rev.* **D57** (1998) 3051.
[62] see also the concept of “fracture functions” in: L. Trentadue, G. Veneziano, *Phys. Lett.* **B323** (1994) 201.
[63] H1 Collab., C. Adloff et al., *Zeit. Phys.* **C74** (1997) 221.
[64] ZEUS Collab., J. Breitweg et al., *Zeit. Phys.* **C75** (1997) 421.
[65] H. Abramowicz, A. Levy, hep-ph/9712415.
[66] ZEUS Coll., M. Derrick et al., *Phys. Lett.* **B356** (1995) 129.
[67] L. Alvero et al., *Phys. Rev.* **D59** (1999) 074022.
[68] H1 Coll., C. Adloff et al., *Eur. Phys. J.* **C1** (1998) 495; *Phys. Lett.* **B428** (1998) 206; *Eur. Phys. J.* **C5** (1998) 439.
[69] ZEUS Coll., paper 505 subm. to this conf.; J. Breitweg et al., *Phys. Lett.* **B421** (1998) 368.
[70] ZEUS Coll., J. Breitweg et al., *Eur. Phys. J.* **C5** (1998) 41.
[71] H1 Coll., C. Adloff et al., *Eur. Phys. J.* **C6** (1999) 421.
[72] H1 Coll., paper 157ae subm. to this conf.
[73] ZEUS Coll., paper 527 subm. to this conf.
[74] H1 Coll., paper 157ag subm. to this conf.
[75] UA8 Coll., A. Brandt et al., *Phys. Lett.* **B297** (1992) 417.
[76] G. Ingelman, P. Schlein, *Phys. Lett.* **B152** (1985) 256.
[77] G. Snow, these proc.
[78] CDF Coll., F. Abe et al., *Phys. Rev. Lett.* **79** (1997) 2636.
[79] D0 Coll., paper 163b subm. to this conf.
[80] CDF Coll., F. Abe et al., *Phys. Rev. Lett.* **78** (1997) 2698.
[81] See e.g. K. Borras (CDF Coll.), proc. of the 7th Int. Workshop on DIS and QCD, Zeuthen (1999).
[82] CDF Coll., T. Affolder et al., subm. to *Phys. Rev. Lett.*
[83] For a summary, see e.g. K. Goulianos, proc. of the 36th Rencontre de Moriond (1999).
[84] CDF Coll., F. Abe et al., *Phys. Rev. Lett.* **80** (1998) 1156; *Phys. Rev. Lett.* **81** (1998) 5278; S. Abachi et al., *Phys. Lett.* **B440** (1998) 189.
[85] V. Del Duca, W.K. Tang, *Phys. Lett.* **B312** (1993) 225.
[86] P. Bruni, G. Ingelman, preprint DESY-93-187.
[87] L. Alvero, J.C. Collins, J.J. Whitmore, hep-ph/9806340.
[88] J. Bjorken, *Phys. Rev.* **D47** (1993) 101; J.C. Collins, L. Frankfurt, M. Strikman, *Phys. Lett.* **B307** (1993) 161; E. Gostman, E. Levin and U. Maor, *Phys. Lett.* **B309** (1993) 199.
[89] L.L. Frankfurt, A. Freund, M. Strikman, *Phys. Rev.* **D58** (1998) 114001; *Phys. Rev.* **D59** (1999) 119901E.
[90] ZEUS Coll., paper subm. to this conf.; P. Saull (ZEUS Coll.), these proc.
[91] see e.g. A. Freund, proc. of the 7th Int. Workshop on DIS and QCD, Zeuthen (1999); K. Golec-Biernat et al., ibid.
[92] P. Marage, proc. of the 28th Int. Symp. on Multipart. Dynamics, Delphi (1998), hep-ph/9904255.
[93] B. Clerbaux, hep-ph/9908519.
[94] J. Ciborowski, these proc.
[95] H1 Coll., C. Adloff et al., preprint DESY-99-010; paper 157n subm. to this conf.
[96] ZEUS Coll., paper 793 subm. to the 29th Int. conf. on HEP, Vancouver (1998).
[97] ZEUS Coll., J. Breitweg et al., preprint DESY-99-102; paper 499 subm. to this conf.
[98] H1 Coll., paper 157aj subm. to this conf.; P. Merkel (H1 Coll.), these proc.
[99] L. Frankfurt, W. Koepf, M. Strikman, *Phys. Rev.* **D54** (1996) 3194; *Phys. Rev.* **D57** (1998) 512.
[100] S.J. Brodsky et al., *Phys. Rev.* **D50** (1994) 3134.
[101] see e.g. M.F. McDermott, proc. of the 7th Int. Workshop on DIS and QCD, Zeuthen (1999); T. Teubner,ibid.
[102] A. Donnachie, P.V. Landshoff, *Phys. Lett.* **B347** (1998) 408.
[103] D.Yu. Ivanov, R. Kirschner, *Phys. Rev.* **D59** (1998) 114026; E.V. Kuraev, N.N. Nikolaev, B.G. Zakharov, *JETP Lett.* **68** (1998) 696; I. Royen, J.-R. Cudell, *Nucl. Phys.* **B545** (1999) 505.

[104] D. Schildknecht, G.A. Schuler, B. Surrow, *Phys. Lett.* **B449** (1999) 328.
[105] A.H. Mueller, proc. of the 6th Int. Workshop on DIS and QCD, Brussels (1998); hep-ph/9911289.
[106] E. Gostman, E. Levin, U. Maor, *Nucl. Phys.* **B493** (1997) 354; *Phys. Lett.* **B425** (1998) 369.
[107] B.Z. Kopeliovich, B. Povh, E. Predazzi, *Phys. Lett.* **B405** (1997) 361.
[108] K. Golec-Biernat, M. Wüsthoff, *Phys. Rev.* **D59** (1999) 014017; hep-ph/9903358.
[109] U. Amaldi, G. Schubert, *Nucl. Phys.* **B166** (1980) 301.
[110] K. Goulianos, J. Montanha, *Phys. Rev.* **D59** (1999) 114017.